Chinese Journal of Physics 78 (2022) 180–193

Contents lists available at ScienceDirect

Chinese Journal of Physics

journal homepage: www.sciencedirect.com/journal/chinese-journal-of-physics

Hybrid nanofluid stagnation point flow past a slip shrinking Riga plate

Nur Syahirah Wahid [a,*], Norihan Md Arifin [a,b], Najiyah Safwa Khashi'ie [c], Ioan Pop [d], Norfifah Bachok [a,b], Mohd Ezad Hafidz Hafidzuddin [e]

[a] Department of Mathematics and Statistics, Faculty of Science Universiti Putra Malaysia, 43400 UPM Serdang, Selangor, Malaysia
[b] Institute for Mathematical Research, Universiti Putra Malaysia, 43400 UPM, Serdang, Selangor, Malaysia
[c] Fakulti Teknologi Kejuruteraan Mekanikal dan Pembuatan, Universiti Teknikal Malaysia Melaka, Hang Tuah Jaya, 76100 Durian Tunggal, Melaka, Malaysia
[d] Department of Mathematics, Babeş-Bolyai University, Cluj-Napoca, R-400084 Romania
[e] Centre of Foundation Studies for Agricultural Science, Universiti Putra Malaysia,43400 UPM Serdang, Selangor, Malaysia

ARTICLE INFO

Keywords:
Hybrid nanofluid
Riga plate
Stagnation point flow
Shrinking
Velocity slip

ABSTRACT

Magnetic nanofluids cover many of uses since their characteristics are externally controllable, and their physical properties may vary with the nanoparticle volume fraction and magnetic field strength. Hybrid nanofluid also has been commercialized as the advancement of traditional nanofluid. The preliminary research on hybrid magnetic nanofluids inspired the present study to discover the stagnation-point flow of hybrid magnetite-cobalt ferrite/water nanofluid towards a shrinking Riga plate with the presence of velocity slip. The complex governing model of the flow is simplified by implementing the similarity transformation. A well-established numerical package, namely bvp4c in MATLAB, is used for numerical calculation as well as stability analysis. Two solutions are found due to the opposing flow from the shrinking Riga plate. From the stability analysis, the first solution which fulfills the boundary condition is the physically stable solution. The rising values of electromagnetohydrodynamic (EMHD) parameter and cobalt ferrite concentration augment the skin friction coefficient. Specifically, the critical point is lessened by 3% when the EMHD parameter is augmented from 0.3 to 0.5 and 0.5 to 0.7, which concludes that a suitably higher EMHD parameter could prevent the separation of the boundary layer. The heat transfer progress is actively performed with the enhancement of EMHD and velocity slip parameters which conclusively shows the suitability of these parameters in developing the cooling heat transfer fluid.

1. Introduction

Heat transfer technologies with high performance are required in many industrial applications especially for cooling or heating. However, these technologies are restricted by the poor thermal conductivity of classical heat transfer fluids, i.e., oil, water, and ethylene glycol. To overcome this challenge, Choi and Eastman [1] created a new innovative fluid known as "nanofluid" by integrating the classical fluids with nanosized solid particles that have strong thermal conductivity [2,3]. Besides, like nanofluid, magnetic

* Corresponding author.
E-mail address: nursyahirahwahid95@yahoo.com (N.S. Wahid).

https://doi.org/10.1016/j.cjph.2022.05.016
Received 12 May 2022; Received in revised form 18 May 2022; Accepted 24 May 2022
Available online 26 May 2022

Nomenclature

a, c	constants
A	velocity slip parameter
A_1	velocity slip factor
C_f	skin friction coefficient
d	electrodes and magnets related parameter
l	characteristic length of the plate
$\overline{M}_0$	magnet magnetization
Nu_x	local Nusselt number
Pr	Prandtl number
Q	electromagnetohydrodynamic parameter
Re_x	local Reynolds number
S	suction/injection parameter
t	time (s)
T	temperature of hybrid nanofluid
T_w	surface temperature
T_∞	ambient temperature
u, v	velocities in x, y directions
x, y	Cartesian coordinates
λ	shrinking parameter
μ_{hnf}	dynamics viscosity of hybrid nanofluid
k_{hnf}	thermal conductivity of hybrid nanofluid $(\mathrm{W/mK})$
ρ_{hnf}	density of hybrid nanofluid $(\mathrm{kg/m^3})$
$(C_p)_{hnf}$	specific heat capacity of hybrid nanofluid $(\mathrm{J/kgK})$
τ	dimensionless time variable
φ_1, φ_2	volume fraction for first and second nanoparticles

nanofluid (ferrofluid) is a mixture of magnetic nanoparticles (ferromagnetic particles) with a diameter of about 10 nanometers that are held together by surfactants in the classical heat transfer fluid [4]. The most exciting feature of magnetic nanofluid is its capacity to produce a broad range of viscosity in a fraction of a millisecond [5]. Additionally, in the existence of a magnetic field, this fluid becomes highly magnetized and may show exceptionally substantial increases in thermal conductivity [6]. Due to the unusual and intriguing features, magnetic nanofluid and magnetic hybrid nanofluid have been used in a broad range of technical applications such as in lubrication, biomedical, and thermal engineering [7–9]. It was reported by various thorough reviews on nanofluids that two models of nanofluids have been continually employed by researchers to solve the flow problem. These models include the Buongiorno model [10–17] and the Tiwari and Das model [18–22], both of which have distinct mechanisms.

Unfortunately, a suspension of mono nanoparticles is insufficient to provide the needed thermal performance. Because of this, "hybrid nanofluid" is introduced to attain the desired thermal characteristic. According to scientific studies, due to the greater thermal conductivity, hybrid nanofluid may be utilized to replace the mono nanofluid, particularly in the automotive, refrigeration systems, photovoltaic modules, electro-mechanical, industrial process, and solar energy industries [23–25]. Sundar et al. [26] stated that the 0.3 vol% water-based hybrid MWCNT-Fe_3O_4 nanofluid has a dynamic viscosity that is 1.5 times greater than the base fluid at room temperature. Besides, the thermal conductivity is also improved for about 13.88% and 28.46% compared to that of base fluid at 20 and 60 °Celsius of operating temperature, respectively. Chu et al. [27] explored the thermal attributes of MWCNT-Fe_3O_4/water nanofluid in a permeable cavity with magnetization. Giwa et al. [28] investigated the heat transmission properties of aqueous Fe_2O_3-Al_2O_3 (75:25) nanofluid in a rectangular cavity. They observed that the heat transmission of 0.1 vol% hybrid nanofluid could be improved when a magnetic field is incorporated. The scrutinization of the magnetohydrodynamic dissipative hybrid Fe_3O_4—$CoFe_2O_4$/ethylene glycol ferrofluid flow has been performed by Tlili et al. [29] with the integration of radiation and heat source/sink. Recently, Anuar et al. [30] researched the flow of hybrid nanofluid due to stagnation point flow on a stretch/shrink surface. Such other recent investigations towards hybrid nanofluids with interesting flow geometry and a variety of effects are conducted by the following researchers: Talebi Rostami et al. [31], Hosseinzadeh et al. [32–37], Salehi et al. [38], Gholinia et al. [39], Wahid et al. [40–43].

Instead of improving the thermophysical features of the fluid itself, heat transfer enhancement can also be achieved by imposing an external agent. In this regard, Riga plate is one of the external devices that was introduced by Gailitis and Lielausus [44]. This Riga plate is a kind of electromagnetic actuator that comprises a span-wise aligned array of alternating permanent magnets and electrodes installed on a flat surface [45,46]. A wall paralleled Lorentz force can be generated when Riga plate is imposed due to the existence of an electric and magnetic field; thus, efficient flow control can be established. Besides, the Riga plate may be inserted to decrease surface friction and pressure drag by inhibiting boundary layer separation and turbulence generation. [47]. Abbas et al. [48] analyzed the slip flow of a micropolar hybrid nanofluid through a stretched Riga. Ragupathi et al. [49] investigated Fe_3O_4 and Al_2O_3 nanofluids with different base fluids across a Riga plate with a non-uniform heat source/sink; it was found that the skin friction increased with the

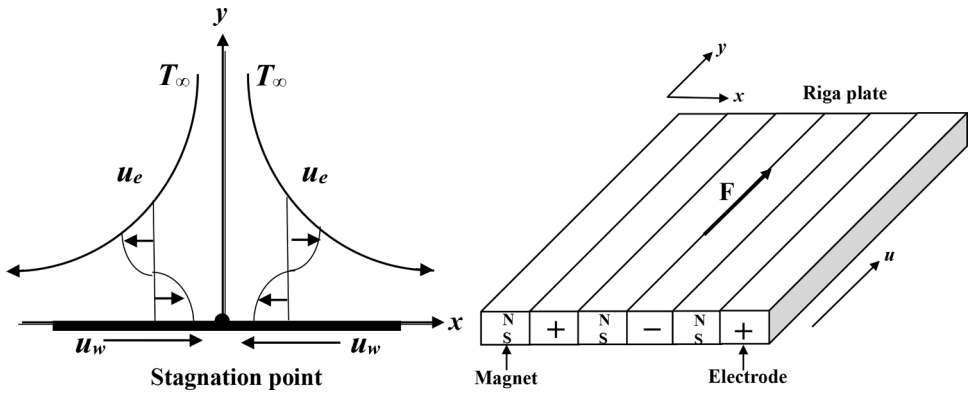

Fig. 1. Physical model.

increased modified Hartman number (EMHD effect). The study of the radiative flow of hybrid nanofluid on a stretched/shrunk Riga plate has been elucidated by Khashi'ie et al. [50]. They reported that the increase in EMHD effect due to the Riga plate helps in delaying the separation process and enhances heat transportation. Most recently, Waqas et al. [51] examined the flow of tangent hyperbolic nanofluid across a Riga plate with second-order velocity slip in the presence of gyrotactic microorganisms.

Moreover, the fluid motion known as stagnation-point flow, which occurs in the stagnation area of a solid surface at the front of a blunt-nosed body, may take place regardless of whether the body is stationary or moving through the fluid. The area around the stagnation point has the greatest pressure and heat transfer rates, as well as the highest mass deposition rates. The concept of stagnation flows was initially presented by Hiemenz [52], and following that, Homann [53] extended the flow analysis to the axisymmetric situation. Moreover, researchers have been interested in the analysis of stagnation point flow that flows past a surface that is either stretching or shrinking. Crane [54] seems to be the first researcher to explore the flow across a linearly stretching surface. In extrusion processes, such as metal sheet extrusion, polymer extrusion, and other manufacturing processes such as glass blowing and plastic film drawing, the boundary layer flow that is influenced by a stretching/shrinking surface is quite important.

According to Goldstein [55], the flow induced by the shrinking surface is basically a reverse/oppose flow. Due to the presence of vorticity inside the boundary layer, as noticed by Wang [56], this form of flow differs from that of the stretched surface. Further, the shrinking/stretching flow of nanofluid with Joule heating was numerically simulated by Hamid et al. [57]. They contemplated that the non-unique solutions are discoverable only for a limited range of shrinking parameter, but the solution is unique for the stretching case. By using the metaheuristic approach, Uddin et al. [58] also found the duality of numerical solutions from the stagnation point flow of nanofluid with magnetic effect past the shrinking sheet problem. Also recently, Khan et al. [59] quantitatively analyzed the aspects of micro-rotation and heat transfer properties of a micropolar hybrid nanofluid flow towards a stagnation point on a stretching/shrinking sheet. They found that the critical value which signifying the separation of the boundary layer was observed to exist in the shrinking sheet region. It can be concluded from these studies that the existence of opposing flow due to the shrinking surface leads to the execution of multiple solutions and it could unveil the point of the flow separation.

In each of the studies described above, most of the flow field was found to comply with the no-slip boundary condition. However, the concept of no-slip condition does not necessarily apply to all physical situations. In certain real-world flow scenarios, the slip boundary condition must be considered for the flow to operate accordingly. Within the realm of industrial applications, slip is used extensively in microscale devices, for instance, in the microelectronic cooling system, the micro heat exchangers, the polishing of artificial heart valves and internal cavities, and the drug delivery system [60–63]. The fluid's flow behavior and shear stress are significantly different when there is a slip at the boundary compared to when there is no slip. In the numerical investigations towards Williamson nanofluid by Hamid et al. [64], the presence of velocity slip is witnessed could reduce the skin friction impact. Meanwhile, during the shrinking flow, the local Nusselt number can be augmented by increasing the velocity slip effect, which has been reported by Wahid et al. [65]. The second-order velocity slip was considered by Abu Bakar et al. [66] in their study towards hybrid nanofluid flow in a porous medium. Abu Bakar et al. [66] noticed the fluid flow is expanded due to the existence of second-order velocity slip. More latest investigations on the boundary layer flow with slip condition are extractable through this reference: [67–71].

Although many numerical investigations have been performed towards hybrid nanofluid flow on a Riga plate, the utilization of magnetic nanoparticles such as magnetite and cobalt ferrite as hybrid nanoparticles is still limited in the literature. Therefore, inspired by the published literature, in this study, we consider the hybrid magnetite-cobalt ferrite/water nanofluid stagnation point flow on a shrinking permeable Riga plate with velocity slip to evaluate its flow properties and heat transfer. The flow problem is modeled mathematically and is solved by using the numerical package known as bvp4c in MATLAB. The stability analysis is also conducted to analyze the feature of the generated numerical dual solutions. Several research questions that we aim to scrutinize in this study are:

(i) Does the flow problem able to generate dual solutions?
(ii) Are the generated numerical solutions stable?
(iii) How can the boundary layer separation be prevented?
(iv) How can the control parameters improve the heat transfer performance?

Table 1
The correlations of the thermophysical properties [76].

Properties	Mono and Hybrid nanofluid
Density	$\rho_{nf} = (1-\varphi)\rho_f + \varphi\rho_s$ $\rho_{hnf} = \rho_{s1}\varphi_1 + \rho_{s2}\varphi_2 + \rho_f(1-\varphi_{hnf})$ where $\varphi_{hnf} = \varphi_1 + \varphi_2$
Heat capacity	$(\rho C_p)_{nf} = (1-\varphi)(\rho C_p)_f + \varphi(\rho C_p)_s$ $(\rho C_p)_{hnf} = (\rho C_p)_{s1}\varphi_1 + (\rho C_p)_{s2}\varphi_2 + (\rho C_p)_f(1-\varphi_{hnf})$
Dynamic viscosity	$\frac{\mu_{nf}}{\mu_f} = \frac{1}{(1-\varphi)^{2.5}}$ $\frac{\mu_{hnf}}{\mu_f} = \frac{1}{(1-\varphi_{hnf})^{2.5}}$
Thermal conductivity	$\frac{k_{nf}}{k_f} = \frac{k_s + 2k_f - 2\varphi(k_f - k_s)}{k_s + 2k_f + \varphi(k_f - k_s)}$ $\frac{k_{hnf}}{k_f} = \left[\frac{2k_f + \left(\frac{\varphi_1 k_{s1} + \varphi_2 k_{s2}}{\varphi_{hnf}}\right) + 2(\varphi_1 k_{s1} + \varphi_2 k_{s2}) - 2\varphi_{hnf}k_f}{2k_f - (\varphi_1 k_{s1} + \varphi_2 k_{s2}) + \left(\frac{\varphi_1 k_{s1} + \varphi_2 k_{s2}}{\varphi_{hnf}}\right) + \varphi_{hnf}k_f}\right]$

(v) How to improve the skin friction by using the considered control parameters?

For a comprehensive evaluation, we have presented the numerical findings in the form of graphs and discussed them thoroughly, while simultaneously answering the research questions.

2. Mathematical model

Consider the hybrid nanofluid stagnation point flow with velocity slip past a shrinking Riga plate, as illustrated in Fig. 1, where the following criteria are considered:

- x and y are the Cartesian coordinates, which the x-axis is parallel to the surface of the plate and the y-axis is perpendicular to the plate with the flow being at the region $y \geq 0$.
- The Riga plate is incorporated of electrodes and magnets with N (North) and S (South) polarities.
- The velocities of the shrinking surface and the ambient (inviscid) fluid is $u_w(x)$ and $u_e(x)$, respectively.
- The velocity of the wall mass transfer across the permeable surface is $v_w(x)$.
- The velocity slip effect is considered with A_1 as the velocity slip factor.
- The constant temperature of the shrinking surface is T_w, and the ambient temperature of the fluid is T_∞.
- The hybrid nanofluid consists of magnetic nanoparticles that are magnetite (Fe3O4) and cobalt ferrite (CoFe2O4), that are dispersed in water (H2O).

According to the abovementioned details, the equations governing the continuity, momentum, and energy together with the boundary conditions are formulated as follows [72–75],

$$\frac{\partial u}{\partial x} + \frac{\partial v}{\partial y} = 0 \tag{1}$$

$$u\frac{\partial u}{\partial x} + v\frac{\partial u}{\partial y} = u_e\frac{\partial u_e}{\partial x} + \frac{\mu_{hnf}}{\rho_{hnf}}\frac{\partial^2 u}{\partial y^2} + \frac{1}{8}\frac{\pi j_0 \overline{M}_0}{\rho_{hnf}}\exp(-y\pi/\alpha_1) \tag{2}$$

$$u\frac{\partial T}{\partial x} + v\frac{\partial T}{\partial y} = \left(\frac{k}{\rho C_p}\right)_{hnf}\frac{\partial^2 T}{\partial y^2} \tag{3}$$

$$v = v_w(x), u = u_w(x) = cx + \frac{\mu_{hnf}}{\rho_{hnf}}A_1\frac{\partial u}{\partial y}, T = T_w, at\ y = 0$$

$$u \to u_e(x) = ax, T \to T_\infty\ as\ y \to \infty \tag{4}$$

Here, u and v are the velocities along x and y axes, respectively, $\overline{M}_0 = (x/l)M_0$ is the magnetization of the permanent magnet where l is the characteristic length of the shrinking plate and M_0 is a constant, T is the temperature of the hybrid nanofluid, $a(>0)$ and c are constants where $c < 0$ for the shrinking plate, and $c = 0$ for the static plate. Moreover, $(\mu, \rho, k, \rho C_p)_{hnf}$ are the dynamics viscosity, density, thermal conductivity, and the heat capacity of the hybrid nanofluid where the correlations are provided in Table 1 (see Takabi and Salehi [76]).

In Table 1, φ is the volume fraction of the magnetic nanoparticles where φ_1 refers to the first nanoparticle and φ_2 refers to the

Table 2
Thermal and physical properties for hybrid nanofluid compositions [79,80].

Properties	ρ(kg /m^3)	C_p(J /kgK)	k(W /mK)	Pr
H_2O	997.1	4179	0.613	6.96
Fe_3O_4	5180	670	9.7	–
$CoFe_2O_4$	4907	700	3.7	–

second nanoparticle. It should be mentioned that if $\varphi_1 = \varphi_2 = 0$, the hybrid nanofluid is simplified to the regular viscous fluid, meanwhile, if either one of them is equal to zero, then the fluid is reduced to the mono nanofluid. The subscripts of hnf, nf, f, s/s1 and s2 in the correlations denote the properties held by hybrid nanofluid, mono nanofluid, base fluid, the first nanoparticle, and the second nanoparticle, respectively (see [76–78]). The respective values for the properties are observable in Table 2 (see also Ahmed et al. [79] and Ul haq et al. [80]).

Guided by the boundary conditions, we propose the following transformation of similarity (see also Bhattacharyya et al. [74]; Nasir et al. [72]):

$$u = axf'(\eta), v = -\sqrt{av_f}f(\eta), \theta(\eta) = \frac{T - T_\infty}{T_w - T_\infty}, \eta = y\sqrt{\frac{a}{v_f}} \tag{5}$$

Applying Eq. (5) into Eqs. (2)-(4), the similarity equations with the related boundary conditions are derived as

$$\left(\frac{\mu_{hnf}/\mu_f}{\rho_{hnf}/\rho_f}\right)f''' - f'^2 + ff'' + 1 + Q\frac{\rho_f}{\rho_{hnf}}\exp(-d\eta) = 0 \tag{6}$$

$$\frac{1}{\Pr}\frac{k_{hnf}/k_f}{(\rho C_p)_{hnf}/(\rho C_p)_f}\theta'' + f\theta' = 0 \tag{7}$$

$$f(0) = S, f'(0) = \lambda + A\left(\frac{\mu_{hnf}/\mu_f}{\rho_{hnf}/\rho_f}\right)f''(0), \theta(0) = 1$$

$$f'(\eta) \to 1, \theta(\eta) \to 0 \, as \, \eta \to \infty \tag{8}$$

The aforementioned equations consist of the following dimensionless parameters: velocity slip parameter $A = A_1\sqrt{a/v_f}$, modified Hartman number or electromagnetohydrodynamic (EMHD) parameter $Q = (\pi j_0 M_0)/(8\rho_f a^2 l)$, the constant shrinking parameter $\lambda = c/a$ with $\lambda < 0$ for shrinking plate and $\lambda = 0$ for static plate, Prandtl number $\Pr = (\nu\rho C_p/k)_f$, the parameter concerning to electrodes and magnets $d = (\pi\sqrt{v_f/a})/\alpha_1$, and the suction/injection parameter $S = -v_w(x)/\sqrt{av_f}$ where $S > 0$ denotes as suction while $S < 0$ denotes as injection.

The skin friction coefficient C_f and the local Nusselt number Nu_x are being considered to analyze the flow and heat transfer properties, such that

$$C_f = \frac{\mu_{hnf}}{\rho_f u_e^2(x)}\left(\frac{\partial u}{\partial y}\right)_{y=0}, Nu_x = \frac{xk_{hnf}}{k_f(T_w - T_\infty)}\left(-\frac{\partial T}{\partial y}\right)_{y=0} \tag{9}$$

Then, applying Eq. (5) into Eq. (9), we obtain

$$C_f \mathrm{Re}_x^{1/2} = \frac{\mu_{hnf}}{\mu_f}f''(0), Nu_x \mathrm{Re}_x^{-1/2} = -\frac{k_{hnf}}{k_f}\theta'(0) \tag{10}$$

where $\mathrm{Re}_x = u_e(x)x/v_f$ is the local Reynolds number.

3. Stability analysis

This present study reveals the generation of non-unique solutions. A stability study is required to discern the practicality of the solutions. The work by Merkin [81] is used as the foundation for this strategy, where the flow model should be time-dependent. Therefore, Eqs. (2) and (3) should be modified into the subsequent form:

$$\frac{\partial u}{\partial t} + u\frac{\partial u}{\partial x} + v\frac{\partial u}{\partial y} = u_e\frac{\partial u_e}{\partial x} + \frac{\mu_{hnf}}{\rho_{hnf}}\frac{\partial^2 u}{\partial y^2} + \frac{\pi j_0 \overline{M}_0}{8\rho_{hnf}}\exp(-y\pi/\alpha_1) \tag{11}$$

$$\frac{\partial T}{\partial t} + u\frac{\partial T}{\partial x} + v\frac{\partial T}{\partial y} = \left(\frac{k}{\rho C_p}\right)_{hnf}\frac{\partial^2 T}{\partial y^2} \tag{12}$$

Table 3
Tabulation and comparison values of $\mathrm{Re}_x^{1/2}C_f$ for different φ_1 of various mono nanofluids when $\varphi_2 = S = A = Q = d = \lambda = 0$.

Φ_1	Present				Khashi'ie et al. [84]	
	Alumina-Water	Copper-Water	Magnetite-Water	Cobalt ferrite-Water	Alumina-Water	Copper-Water
0.05	1.408762990	1.553849594	1.445478750	1.437276883	1.4088	1.5538
0.10	1.602056738	1.884323750	1.675264477	1.659029586	1.6020	1.8843
0.15	1.816825557	2.236903964	1.927699497	1.903248462	1.8168	2.2369
0.20	2.058324536	2.622743104	2.209264659	2.176124357	2.0583	2.6227

where t is time. Then, the new transformation variables are introduced that comes together with the non-dimensional time variable τ, such that:

$$u = ax\frac{\partial f}{\partial \eta}(\eta,\tau), v = -\sqrt{av_f}f(\eta,\tau), \theta(\eta,\tau) = \frac{T-T_\infty}{T_w-T_\infty}, \eta = y\sqrt{\frac{a}{v_f}}, \tau = at \tag{13}$$

Implementing the transformation variables, Eqs. (11) and (12) now become:

$$\left(\frac{\mu_{hnf}/\mu_{hnf}}{\rho_{hnf}/\rho_{hnf}}\right)\frac{\partial^3 f}{\partial \eta^3} + f\frac{\partial^2 f}{\partial \eta^2} + 1 - \left(\frac{\partial f}{\partial \eta}\right)^2 + Q\frac{\rho_f}{\rho_{hnf}}\exp(-d\eta) - \frac{\partial^2 f}{\partial \eta \partial \tau} = 0 \tag{14}$$

$$\frac{1}{\mathrm{Pr}}\frac{k_{hnf}/k_f}{(\rho C_p)_{hnf}/(\rho C_p)_f}\frac{\partial^2 \theta}{\partial \eta^2} + f\frac{\partial \theta}{\partial \eta} - \frac{\partial \theta}{\partial \tau} = 0 \tag{15}$$

conditioned to

$$\begin{aligned} &f(0,\tau) = S, \frac{\partial f}{\partial \eta}(0,\tau) = \lambda + A\left(\frac{\mu_{hnf}/\mu_f}{\rho_{hnf}/\rho_f}\right)\frac{\partial^2 f}{\partial \eta^2}(0,\tau), \theta(0,\tau) = 1, \\ &\frac{\partial f}{\partial \eta}(\infty,\tau) \to 1, \theta(\infty,\tau) \to 0. \end{aligned} \tag{16}$$

Now, as referring to Weidman et al. [82], the following perturbation equations should be applied to the previous equations

$$\begin{aligned} f(\eta,\tau) &= f_0(\eta) + e^{-\gamma\tau}F(\eta,\tau) \\ \theta(\eta,\tau) &= \theta_0(\eta) + e^{-\gamma\tau}G(\eta,\tau) \end{aligned} \tag{17}$$

where γ is the eigenvalue parameter, $F(\eta,\tau)$ and $G(\eta,\tau)$ are the small relatives to $f_0(\eta)$ and $\theta_0(\eta)$, respectively. Hence, after substitution and simplification, we get

$$\left(\frac{\mu_{hnf}/\mu_{hnf}}{\rho_{hnf}/\rho_{hnf}}\right)F''' + f_0F'' + Ff_0'' - 2f_0'F' + \gamma F' = 0 \tag{18}$$

$$\frac{1}{\mathrm{Pr}}\frac{k_{hnf}/k_f}{(\rho C_p)_{hnf}/(\rho C_p)_f}G'' + f_0G' + F\theta_0' + \gamma G = 0 \tag{19}$$

$$\begin{aligned} &F(0) = 0, F'(0) = A\left(\frac{\mu_{hnf}/\mu_f}{\rho_{hnf}/\rho_f}\right)F''(0), G(0) = 0, \\ &F'(\infty) \to 0, G(\infty) \to 0. \end{aligned} \tag{20}$$

Finally, before solving these equations, we chose to relax $F'(\infty) \to 0$ and replace it with $F''(0) = 1$ to ensure the possible smallest eigenvalue γ_1 from the infinite set of eigenvalues $\gamma_1 < \gamma_2 < \gamma_3 \cdots < \gamma_n < \gamma_{n+1}$ can be generated (see Harris et al. [83]). We consider the flow solution to be stable only when the generated smallest eigenvalue is positive $(\gamma_1 > 0)$. This positive smallest eigenvalue will eventually approach zero when $\lambda \to \lambda_c$, signifying that the solution is stable as the applied perturbation decays over time.

4. Results and discussion

The unique qualities of the control parameters covered in the model are discussed in this section. Accordingly, Eqs. (6) to (8) are solved using the bvp4c package in MATLAB with zero (10^{-10}) tolerance error limit, and the numerical results are shown in both figures and tables. We have initially set the boundary layer thickness to be $\eta_\infty = 15$. The volume fraction of the first magnetic nanoparticle (magnetite) is set to be constant throughout the study at the value of $\varphi_1 = 0.01$; meanwhile, the other control parameters such as the volume fraction/concentration of the second nanoparticle (cobalt ferrite), velocity slip parameter, EMHD parameter, and shrinking

Table 4
Comparison values of $\mathrm{Re}_x^{1/2}C_f$ for different λ of various mono nanofluids with $\varphi_1 = 0.1$ when $\varphi_2 = S = A = Q = d = 0$.

λ	Present		Malvandi et al. [85]	
	Alumina-Water	Copper-Water	Alumina-Water	Copper-Water
-0.5	1.943997912	2.286511675	1.94399	2.28651
0	1.602056738	1.884323750	1.60205	1.88432
0.5	0.927105658	1.090452773	0.9271	1.09045

Table 5
Comparison values of $\mathrm{Re}_x^{-1/2}Nu_x$ for different λ of various mono nanofluids with $\varphi_1 = 0.1$ when $\varphi_2 = S = A = Q = d = 0$ and $\mathrm{Pr} = 6.2$.

λ	Present		Malvandi et al. [85]	
	Alumina-Water	Copper-Water	Alumina-Water	Copper-Water
-0.5	0.727148524	0.838510195	0.72714	0.83851
0	1.330508477	1.404327126	1.3305	1.40432
0.5	1.827846874	1.872386445	1.82784	1.87238

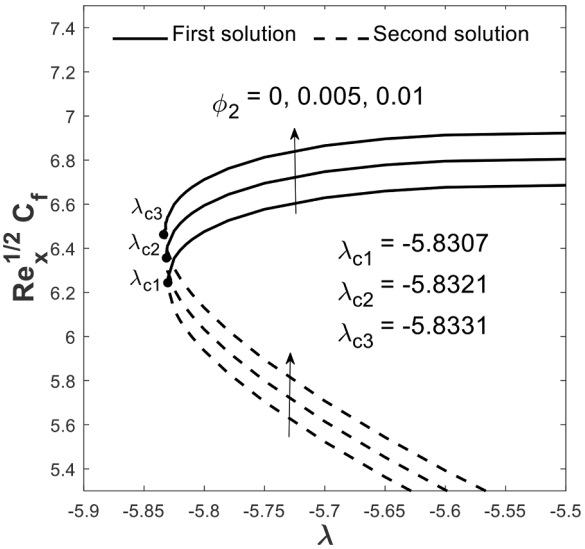

Fig. 2. Plot of $\mathrm{Re}_x^{1/2}C_f$ for varied φ_2 when $\varphi_1 = 0.01$, $A = Q = d = 0.5$ and $S = 2$.

parameter are set to be varied appropriately. It should be noted that these varied values are chosen in accordance with the conformity of the far-field boundary conditions as stated in Eq. (8) and with guidance from the related existing studies. We also have fixed the Prandtl number at the value of 6.96 as recommended by Ahmed et al. [79] unless being stated by another value.

Tables 3, 4 and 5 present the values of $\mathrm{Re}_x^{1/2}C_f$ and $\mathrm{Re}_x^{-1/2}Nu_x$ for the specific limiting cases for various types of mono nanofluids. These values are noticed to be consistent with the existing published results by Khashi'ie et al. [84] and Malvandi [85], which also verifies the validity of the current method and model. The plots of $\mathrm{Re}_x^{1/2}C_f$ and $\mathrm{Re}_x^{-1/2}Nu_x$ versus the shrinking parameter for the assorted values of volume fraction of cobalt ferrite are illustrated in Figs. 2 and 3. These plots show that there exist two different solutions in the domain, and we hypothesized that these dual solutions are generated resulting to the opposing flow provided by the shrinking parameter. Interestingly, the existence of these dual solutions allows us to predict and control the flow separation process that occurs within the layer. In this case, it is evaluated that the increase in volume fraction of cobalt ferrite is necessary to augment the skin friction and delay the flow separation process. However, the opposite pattern is shown for the heat transfer process. Physically, the rise in volume fraction of cobalt ferrite increases the fluid viscosity, which then improves the skin friction across the surface. Also, when cobalt ferrite volume fraction increases, the temperature of the plate rises, hence, lowering the efficiency of thermal conductivity and negatively affecting the heat transfer rate of the fluid.

Figs. 4 and 5 portray the effect of velocity slip parameter towards $\mathrm{Re}_x^{1/2}C_f$and $\mathrm{Re}_x^{-1/2}Nu_x$ at the shrinking domain. Greater skin friction is achievable if a smaller velocity slip is considered for both first and the second solution. Nevertheless, a higher velocity slip is needed to augment the heat transfer progress as predicted by the first solution in Fig. 5. This is because, the increase in velocity slip parameter led to a reduction in flow resistance, which in turn reduces the skin friction. As stated by Mishra and Kumar [86], any form of fluid model that has a velocity slip will have a lower temperature. Thus, this also implies that the heat transfer progress has occurred

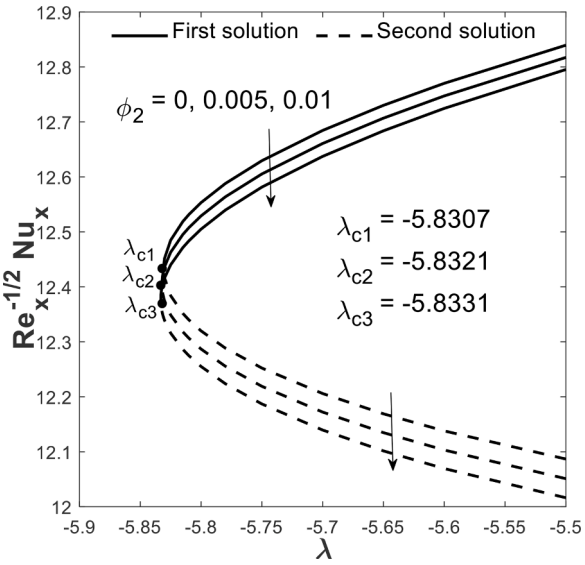

Fig. 3. Plot of $\mathrm{Re}_x^{-1/2}Nu_x$ for varied φ_2 when $\varphi_1 = 0.01$, $A = Q = d = 0.5$ and $S = 2$.

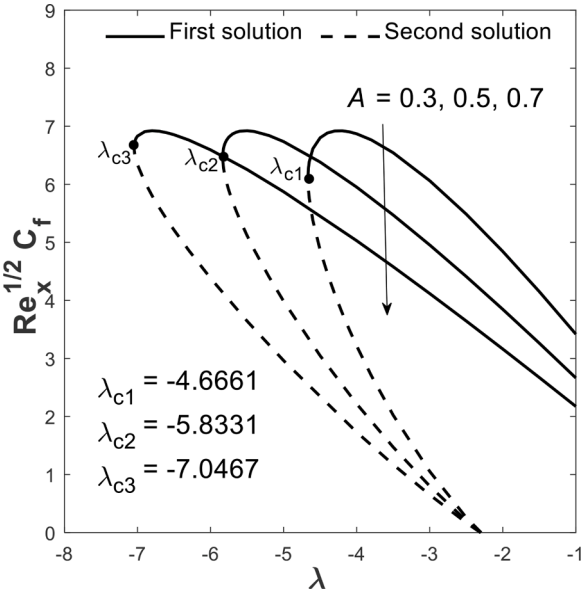

Fig. 4. Plot of $\mathrm{Re}_x^{1/2}C_f$ for varied A when $\varphi_1 = \varphi_2 = 0.01$, $Q = d = 0.5$ and $S = 2$.

very fast when velocity slip is considered. In this case, velocity slip can be used as a cooling agent. Besides, the rise in the velocity slip parameter also has reduced the value of the critical point and widened the domain of the feasible solution. Resultantly, the boundary layer separation process can be detained, and the flow phase can be maintained. From these figures, we notice that the pattern of $\mathrm{Re}_x^{1/2}C_f$ behaves in an increasing manner up to a certain point before it reaches the critical point when the shrinking parameter is reduced, and oppositely for the pattern provided by $\mathrm{Re}_x^{-1/2}Nu_x$. This observation is also valid for other findings in Figs. 2, 3, 6, and 7.

Furthermore, Figs. 6 and 7 display the plots of $\mathrm{Re}_x^{1/2}C_f$and $\mathrm{Re}_x^{-1/2}Nu_x$ at the shrinking domain for different values of EMHD parameter or the (modified) Hartman number. The higher intensity of this parameter could lead to the enhancement of both skin friction and the heat transfer progress for the considered hybrid nanofluid as predicted by the first solution but not for the second solution. Logically, this is because the increment of EMHD parameter increases the Lorentz force strength that causes the flow resistance to increase, which consequently augments the skin friction and enhances the heat transfer. However, we believe the prediction provided by the first solution is more realizable than the second solution, which will later be validated and discussed through the evaluation provided by the stability analysis at the end of this section. Moreover, like the other control parameters, the increment

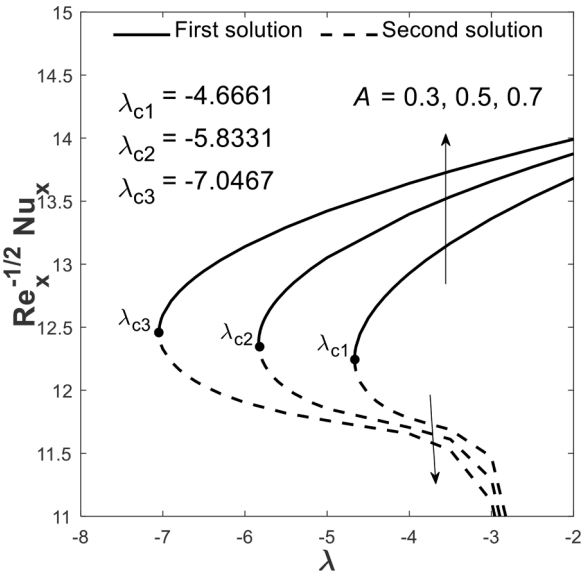

Fig. 5. Plot of $\mathrm{Re}_x^{-1/2} Nu_x$ for varied A when $\varphi_1 = \varphi_2 = 0.01$, $Q = d = 0.5$ and $S = 2$.

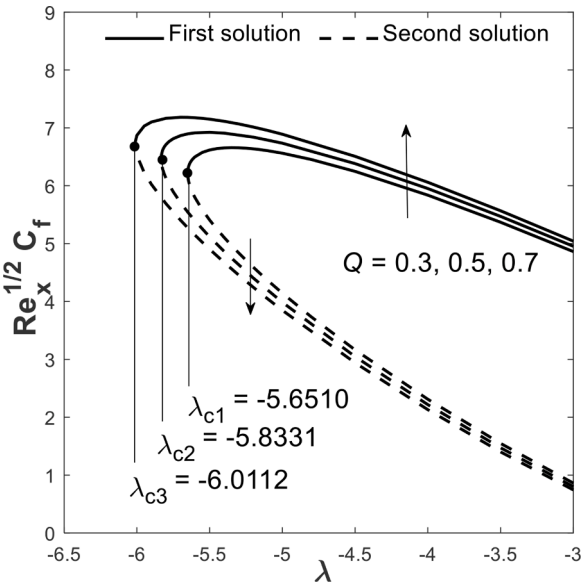

Fig. 6. Plot of $\mathrm{Re}_x^{1/2} C_f$ for varied Q when $\varphi_1 = \varphi_2 = 0.01$, $A = d = 0.5$ and $S = 2$.

of this EMHD parameter could aid in maintaining the flow condition and delay the flow separation process as observed through the generated critical points. This finding is consistent with the basic Riga plate theory, in which the wall Lorentz force is activated to delay the separation of boundary layer flow.

To view the findings from the velocity and temperature perspective, we also graphically presented the respective profiles with the changing values of control parameters, as can be seen in Figs. 8, 9, and 10. Upon contemplation on the first solution, the velocity profile is observed to increase only when the velocity slip and the EMHD parameters are increasing, but adversely for the nanoparticles volume fraction parameter. Logically, the increment of cobalt ferrite volume fraction would increase the viscosity of the fluid due to the increase in the molecular interaction between the hybrid nanoparticles and the base fluid [87], consequently causing the velocity to decrease. Nevertheless, the temperature profile for the first solution is noticed to increase when the velocity slip and EMHD parameters decrease and when the volume fraction of cobalt ferrite increases. The effect of these parameters towards the temperature profile is also supported by the findings on the heat transfer progress, as illustrated in Figs. 3, 5, and 7; where the increment in these control parameters leads to the escalation of heat transfer, which would eventually causes the temperature profile to decrease.

For the stability analysis, the finding is provided in Fig. 11 through the plot of the smallest eigenvalue versus the shrinking

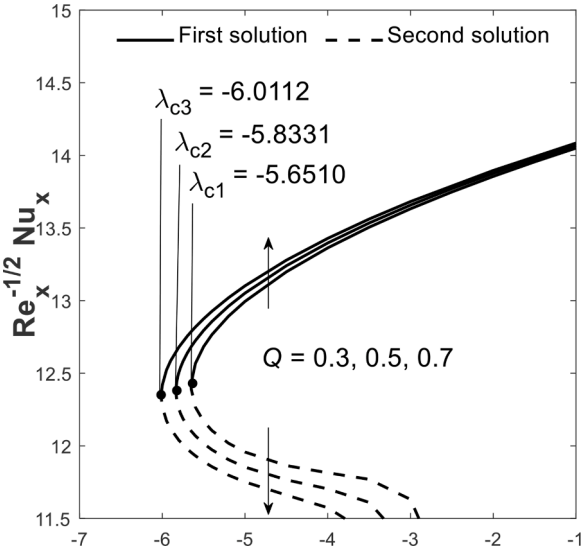

Fig. 7. Plot of $\mathrm{Re}_x^{-1/2} Nu_x$ for varied Q when $\varphi_1 = \varphi_2 = 0.01$, $A = d = 0.5$ and $S = 2$.

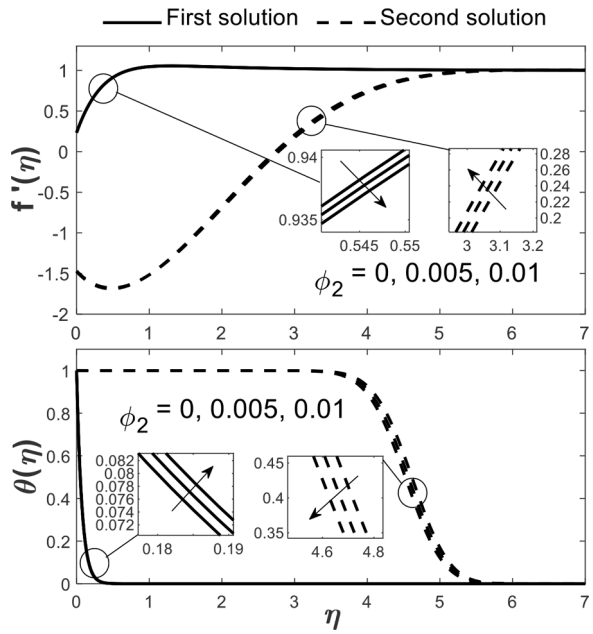

Fig. 8. $f'(\eta)$ and $\theta(\eta)$ for varied φ_2 when $\varphi_1 = 0.01$, $A = Q = d = 0.5$ and $S = 2$.

parameter within the selected condition. The first solution generates the positive value of γ_1 whereas the second solution generates the negative value of γ_1 as the shrinking parameter (λ) approaches the critical value $\lambda_c = -5.8331$. Hence, this implies the first solution to be the only real solution in this study. This conclusion is justified by the trend provided by γ_1 when $\lambda \to \lambda_c$ where it shows that γ_1 will eventually approach towards zero which notifies the decay and the growth of the perturbation. Therefore, the solution is considered real and stable when the perturbation is decayed as time evolves (shown by the first solution).

5. Conclusions

The mathematical model of magnetic hybrid nanofluid stagnation point flow past a shrinking Riga plate with velocity slip is scrutinized numerically in this study. The influence of the control parameters, namely velocity slip, EMHD, volume fraction, and shrinking parameter, are evaluated towards the physical quantities and the related profiles. The key findings from this study are concluded as follows:

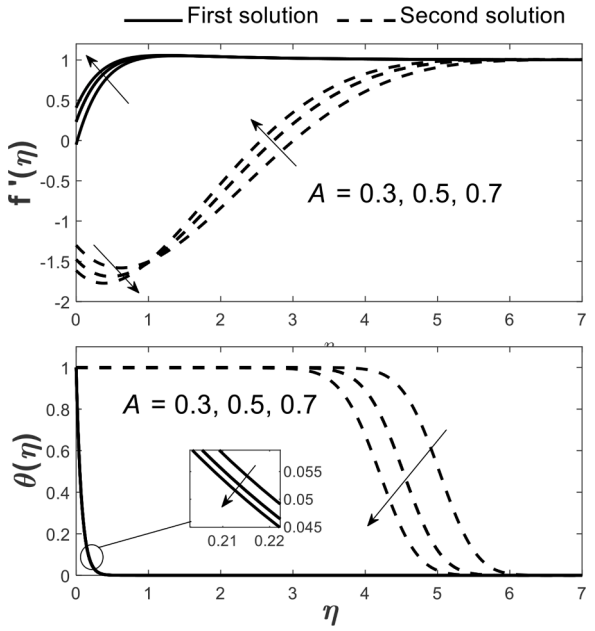

Fig. 9. $f'(\eta)$ and $\theta(\eta)$ for varied A when $\varphi_1 = \varphi_2 = 0.01$, $Q = d = 0.5$ and $S = 2$.

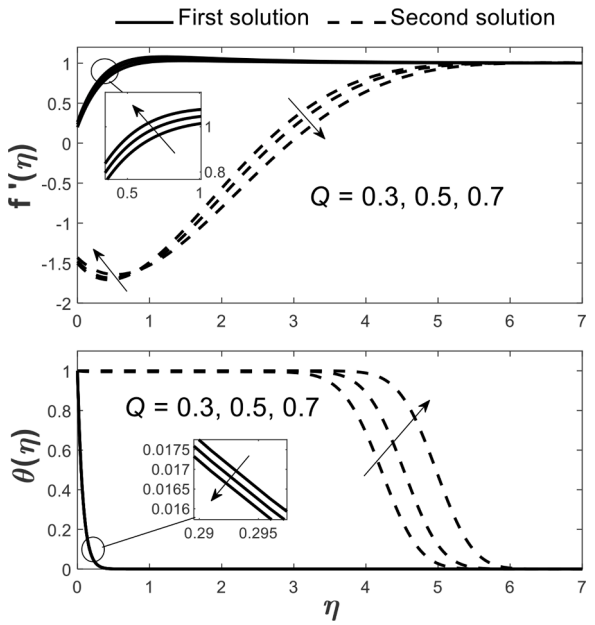

Fig. 10. $f'(\eta)$ and $\theta(\eta)$ for varied Q when $\varphi_1 = \varphi_2 = 0.01$, $A = d = 0.5$ and $S = 2$.

- Two different solutions are computed, and the second solution is not admissible.
- The skin friction is improved when a greater volume fraction of cobalt ferrite is applied but adversely for the velocity slip and EMHD parameters.
- The heat transfer progress is augmented when velocity slip and EMHD parameters are applied but adversely for the volume fraction of cobalt ferrite.
- The existence of velocity slip and EMHD parameters can be used as the cooling agent.
- The fluid velocity can be sped up by the gradual addition of velocity slip and EMHD parameters.

The model formulation and findings of this study are essential and may be used as guidance, especially for the researchers in nanofluids. Other parameters such as viscous dissipation, melting, and Joule heating can be considered for a deeper analysis in future

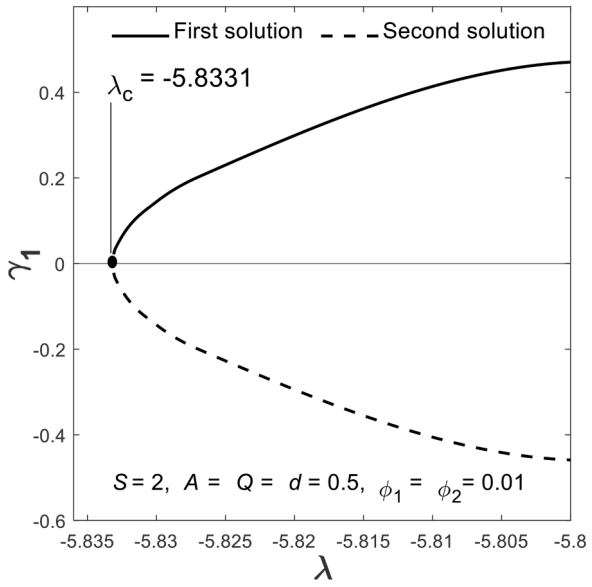

Fig. 11. Plot of the smallest eigenvalues for varied shrinking parameter.

studies. The implementation of other types of magnetic nanoparticles and base fluids is also encouraged. Despite the fact that this is a theoretical research, it is also highly encouraged that an experimental analysis of this flow problem is conducted as well for future research.

Declaration of Competing Interest

The authors declare that they have no known competing financial interests or personal relationships that could have appeared to influence the work reported in this paper.

Acknowledgement

The authors acknowledge Universiti Putra Malaysia, Universiti Teknikal Malaysia Melaka, and the Ministry of Higher Education Malaysia for the Fundamental Research Grant Scheme (KPTFRGS/1/2019/STG06/IPM/02/3, Vot 5540309).

References

[1] S.U.S. Choi, J.A. Eastman, Enhancing thermal conductivity of fluids with nanoparticles, ASME Fluids Eng. Division 231 (1995) 99–106.
[2] J. Li, X. Zhang, B. Xu, M. Yuan, Nanofluid research and applications: a review, Int. Commun. Heat and Mass Transf. 127 (2021) 105543. 10.1016/j.icheatmasstransfer.2021.105543.
[3] R. Lenin, P.A. Joy, C. Bera, A review of the recent progress on thermal conductivity of nanofluid, J. Mol. Liq. 338 (2021), 116929, https://doi.org/10.1016/j.molliq.2021.116929.
[4] R.E. Rosensweig, Ferrofluids: introduction. Reference Module in Materials Science and Materials Engineering, Elsevier, 2016, B9780128035818025000, https://doi.org/10.1016/B978-0-12-803581-8.02477-2.
[5] S. Genc, B. Derin, Synthesis and rheology of ferrofluids: a review, Curr. Opin. Chem. Eng. 3 (2014) 118–124, https://doi.org/10.1016/j.coche.2013.12.006.
[6] W.A. Khan, Z.H. Khan, R.U. Haq, Flow and heat transfer of ferrofluids over a flat plate with uniform heat flux, Eur. Phys. J. Plus. 130 (2015) 86, https://doi.org/10.1140/epjp/i2015-15086-4.
[7] M. Kole, S. Khandekar, Engineering applications of ferrofluids: a review, J. Magn. Magn. Mater. 537 (2021), 168222, https://doi.org/10.1016/j.jmmm.2021.168222.
[8] H. Shokrollahi, Structure, synthetic methods, magnetic properties and biomedical applications of ferrofluids, Mater. Sci. Eng. C 33 (2013) 2476–2487, https://doi.org/10.1016/j.msec.2013.03.028.
[9] M.A. Khairul, E. Doroodchi, R. Azizian, B. Moghtaderi, Advanced applications of tunable ferrofluids in energy systems and energy harvesters: a critical review, Energy Conversion and Manag. 149 (2017) 660–674, https://doi.org/10.1016/j.enconman.2017.07.064.
[10] J. Buongiorno, Convective transport in nanofluids, J. Heat Transf. 128 (2006) 240–250, https://doi.org/10.1115/1.2150834.
[11] A.Hamid Hashim, M. Khan, Unsteady mixed convective flow of Williamson nanofluid with heat transfer in the presence of variable thermal conductivity and magnetic field, J. Mol. Liq. 260 (2018) 436–446, https://doi.org/10.1016/j.molliq.2018.03.079.
[12] A. Hamid, M.Khan Hashim, Impacts of binary chemical reaction with activation energy on unsteady flow of magneto-Williamson nanofluid, J. Mol. Liq. 262 (2018) 435–442, https://doi.org/10.1016/j.molliq.2018.04.095.
[13] A.Hamid Hashim, M. Khan, Heat and mass transport phenomena of nanoparticles on time-dependent flow of Williamson fluid towards heated surface, Neural Comput. Appl. 32 (2020) 3253–3263, https://doi.org/10.1007/s00521-019-04100-4.
[14] A. Hamid, M.Alghamdi Hashim, M. Khan, A.S. Alshomrani, An investigation of thermal and solutal stratification effects on mixed convection flow and heat transfer of Williamson nanofluid, J. Mol. Liq. 284 (2019) 307–315, https://doi.org/10.1016/j.molliq.2019.03.181.
[15] A. Hamid, Existence of dual solutions for wedge flow of magneto-Williamson nanofluid: a revised model, Alexandria Eng. J. 59 (2020) 1525–1537, https://doi.org/10.1016/j.aej.2020.04.001.

[16] Kh. Hosseinzadeh, So. Roghani, A.R. Mogharrebi, A. Asadi, M. Waqas, D.D. Ganji, Investigation of cross-fluid flow containing motile gyrotactic microorganisms and nanoparticles over a three-dimensional cylinder, Alexandria Eng. J. 59 (2020) 3297–3307, https://doi.org/10.1016/j.aej.2020.04.037.
[17] Kh. Hosseinzadeh, S. Salehi, M.R. Mardani, F.Y. Mahmoudi, M. Waqas, D.D. Ganji, Investigation of nano-Bioconvective fluid motile microorganism and nanoparticle flow by considering MHD and thermal radiation, Inf. Med. Unlocked 21 (2020), 100462, https://doi.org/10.1016/j.imu.2020.100462.
[18] R.K. Tiwari, M.K. Das, Heat transfer augmentation in a two-sided lid-driven differentially heated square cavity utilizing nanofluids, Int. J. Heat Mass Transf. 50 (2007) 2002–2018, https://doi.org/10.1016/j.ijheatmasstransfer.2006.09.034.
[19] S. Dinarvand, I. Pop, Free-convective flow of copper/water nanofluid about a rotating down-pointing cone using Tiwari-Das nanofluid scheme, Adv. Powder Technol. 28 (2017) 900–909, https://doi.org/10.1016/j.apt.2016.12.016.
[20] E.A. Sayed, M. Fathy, Numerical study of flow and heat transfer of a nanofluid past a vertical cone, Case Stud. Therm. Eng. 34 (2022), 102038, https://doi.org/10.1016/j.csite.2022.102038.
[21] A. Ur Rehman, Z. Abbas, Stability analysis of heat transfer in nanomaterial flow of boundary layer towards a shrinking surface: hybrid nanofluid versus nanofluid, Alexandria Eng. J. 61 (2022) 10757–10768, https://doi.org/10.1016/j.aej.2022.04.020.
[22] M. Aghamajidi, M. Yazdi, S. Dinarvand, I. Pop, Tiwari-Das nanofluid model for magnetohydrodynamics (MHD) natural-convective flow of a nanofluid adjacent to a spinning down-pointing vertical cone, Propulsion and Power Res. 7 (2018) 78–90, https://doi.org/10.1016/j.jppr.2018.02.002.
[23] D.P. Kshirsagar, M.A. Venkatesh, A review on hybrid nanofluids for engineering applications, Mater. Today: Proceedings 44 (2021) 744–755, https://doi.org/10.1016/j.matpr.2020.10.637.
[24] M. Muneeshwaran, G. Srinivasan, P. Muthukumar, C.-.C. Wang, Role of hybrid-nanofluid in heat transfer enhancement – A review, Int. Commun. Heat and Mass Transf. 125 (2021), 105341, https://doi.org/10.1016/j.icheatmasstransfer.2021.105341.
[25] J.P. Vallejo, J.I. Prado, L. Lugo, Hybrid or mono nanofluids for convective heat transfer applications. A critical review of experimental research, Appl. Therm. Eng. 203 (2022), 117926, https://doi.org/10.1016/j.applthermaleng.2021.117926.
[26] L.S. Sundar, M.K. Singh, A.C.M. Sousa, Enhanced heat transfer and friction factor of MWCNT–Fe3O4/water hybrid nanofluids, Int. Commun. Heat and Mass Transf. 52 (2014) 73–83, https://doi.org/10.1016/j.icheatmasstransfer.2014.01.012.
[27] Y. Chu, S. Bilal, M.R. Hajizadeh, Hybrid ferrofluid along with MWCNT for augmentation of thermal behavior of fluid during natural convection in a cavity, Math. Meth. Appl. Sci. (2020) 6937, https://doi.org/10.1002/mma.6937, mma.
[28] S.O. Giwa, M. Sharifpur, J.P. Meyer, Effects of uniform magnetic induction on heat transfer performance of aqueous hybrid ferrofluid in a rectangular cavity, Appl. Therm. Eng. 170 (2020), 115004, https://doi.org/10.1016/j.applthermaleng.2020.115004.
[29] I. Tlili, M.T. Mustafa, K.A. Kumar, N. Sandeep, Effect of asymmetrical heat rise/fall on the film flow of magnetohydrodynamic hybrid ferrofluid, Sci. Rep. 10 (2020) 6677, https://doi.org/10.1038/s41598-020-63708-y.
[30] N.S. Anuar, N. Bachok, I. Pop, Influence of MHD hybrid ferrofluid flow on exponentially stretching/shrinking surface with heat source/sink under stagnation point region, Mathematics 9 (2021) 2932, https://doi.org/10.3390/math9222932.
[31] H. Talebi Rostami, M. Fallah Najafabadi, Kh. Hosseinzadeh, D.D. Ganji, Investigation of mixture-based dusty hybrid nanofluid flow in porous media affected by magnetic field using RBF method, Int. J. Ambient Energy (2022) 1–11, https://doi.org/10.1080/01430750.2021.2023041.
[32] S. Hosseinzadeh, Kh. Hosseinzadeh, A. Hasibi, D.D. Ganji, Thermal analysis of moving porous fin wetted by hybrid nanofluid with trapezoidal, concave parabolic and convex cross sections, Case Stud. Therm. Eng. 30 (2022), 101757, https://doi.org/10.1016/j.csite.2022.101757.
[33] Kh. Hosseinzadeh, M.R. Mardani, S. Salehi, M. Paikar, D.D. Ganji, Investigation of micropolar hybrid nanofluid (Iron Oxide–Molybdenum Disulfide) flow across a sinusoidal cylinder in presence of magnetic field, Int. J. Appl. Comput. Math. 7 (2021) 210, https://doi.org/10.1007/s40819-021-01148-6.
[34] K. Hosseinzadeh, M.R. Mardani, S. Salehi, M. Paikar, M. Waqas, D.D. Ganji, Entropy generation of three-dimensional Bödewadt flow of water and hexanol base fluid suspended by Fe3O4 and MoS2 hybrid nanoparticles, Pramana - J. Phys. 95 (2021) 57, https://doi.org/10.1007/s12043-020-02075-9.
[35] Kh. Hosseinzadeh, So. Roghani, A.R. Mogharrebi, A. Asadi, D.D. Ganji, Optimization of hybrid nanoparticles with mixture fluid flow in an octagonal porous medium by effect of radiation and magnetic field, J. Therm. Anal. Calorim 143 (2021) 1413–1424, https://doi.org/10.1007/s10973-020-10376-9.
[36] Kh. Hosseinzadeh, A. Asadi, A.R. Mogharrebi, M. Ermia Azari, D.D. Ganji, Investigation of mixture fluid suspended by hybrid nanoparticles over vertical cylinder by considering shape factor effect, J. Therm. Anal. Calorim 143 (2021) 1081–1095, https://doi.org/10.1007/s10973-020-09347-x.
[37] Kh. Hosseinzadeh, E. Montazer, M.B. Shafii, D.D. Ganji, Heat transfer hybrid nanofluid (1-Butanol/MoS2–Fe 3O4) through a wavy porous cavity and its optimization, HFF 31 (2021) 1547–1567, https://doi.org/10.1108/HFF-07-2020-0442.
[38] Sajad. Salehi, Amin. Nori, Kh. Hosseinzadeh, D.D. Ganji, Hydrothermal analysis of MHD squeezing mixture fluid suspended by hybrid nanoparticles between two parallel plates, Case Stud. Therm. Eng. 21 (2020), 100650, https://doi.org/10.1016/j.csite.2020.100650.
[39] M. Gholinia, Kh. Hosseinzadeh, D.D. Ganji, Investigation of different base fluids suspend by CNTs hybrid nanoparticle over a vertical circular cylinder with sinusoidal radius, Case Stud. Therm. Eng. 21 (2020), 100666, https://doi.org/10.1016/j.csite.2020.100666.
[40] N.S. Wahid, N. Md Arifin, M. Turkyilmazoglu, M.E.H. Hafidzuddin, N.A Abd Rahmin, MHD Hybrid Cu-Al2O3/Water nanofluid flow with thermal radiation and partial slip past a permeable stretching surface: analytical solution, JNanoR 64 (2020) 75–91, https://doi.org/10.4028/www.scientific.net/JNanoR.64.75.
[41] N.S. Wahid, N.M. Arifin, N.S. Khashi'ie, R.I. Yahaya, I. Pop, N. Bachok, M.E.H. Hafidzuddin, Three-dimensional radiative flow of hybrid nanofluid past a shrinking plate with suction, ARFMTS 85 (2021) 54–70, https://doi.org/10.37934/arfmts.85.1.5470.
[42] N.S. Wahid, N.M. Arifin, N.S. Khashi'ie, I. Pop, N. Bachok, M.E.H. Hafidzuddin, Flow and heat transfer of hybrid nanofluid induced by an exponentially stretching/shrinking curved surface, Case Stud. Therm. Eng. 25 (2021), 100982, https://doi.org/10.1016/j.csite.2021.100982.
[43] N.S. Wahid, N. Md Arifin, N.S. Khashi'ie, I. Pop, N. Bachok, M.E.H. Hafidzuddin, MHD mixed convection flow of a hybrid nanofluid past a permeable vertical flat plate with thermal radiation effect, Alexandria Eng. J. 61 (2022) 3323–3333, https://doi.org/10.1016/j.aej.2021.08.059.
[44] A. Gailitis, O. Lielausus, On a possibility to reduce the hydrodynamic resistance of a plate in an electrolyte, Appl. Magnetohydrodynamic. 12 (1961) 143–146.
[45] R. Ahmad, M. Mustafa, M. Turkyilmazoglu, Buoyancy effects on nanofluid flow past a convectively heated vertical Riga-plate: a numerical study, Int. J. Heat Mass Transf. 111 (2017) 827–835, https://doi.org/10.1016/j.ijheatmasstransfer.2017.04.046.
[46] E. Magyari, A. Pantokratoras, Aiding and opposing mixed convection flows over the Riga-plate, Commun. Nonlinear Sci. Numerical Simulation 16 (2011) 3158–3167, https://doi.org/10.1016/j.cnsns.2010.12.003.
[47] N.V. Ganesh, Q.M. Al-Mdallal, S. Al Fahel, S. Dadoa, Riga – Plate flow of γ Al2O3-water/ethylene glycol with effective Prandtl number impacts, Heliyon 5 (2019) e01651, https://doi.org/10.1016/j.heliyon.2019.e01651.
[48] N. Abbas, S. Nadeem, M.Y. Malik, Theoretical study of micropolar hybrid nanofluid over Riga channel with slip conditions, Physica A: Statistical Mech. Its Appl. 551 (2020), 124083, https://doi.org/10.1016/j.physa.2019.124083.
[49] P. Ragupathi, A.K.A. Hakeem, Q.M. Al-Mdallal, B. Ganga, S. Saranya, Non-uniform heat source/sink effects on the three-dimensional flow of Fe3O4/Al2O3 nanoparticles with different base fluids past a Riga plate, Case Stud. Therm. Eng. 15 (2019), 100521, https://doi.org/10.1016/j.csite.2019.100521.
[50] N.S. Khashi'ie, N.M. Arifin, M. Sheremet, I. Pop, Shape factor effect of radiative Cu–Al2O3/H2O hybrid nanofluid flow towards an EMHD plate, Case Stud. Therm. Eng. 26 (2021) 101199. 10.1016/j.csite.2021.101199.
[51] H. Waqas, A. Kafait, T. Muhammad, U. Farooq, Numerical study for bio-convection flow of tangent hyperbolic nanofluid over a Riga plate with activation energy, Alexandria Eng. J. 61 (2022) 1803–1814, https://doi.org/10.1016/j.aej.2021.06.068.
[52] K. Hiemenz, Die Grenzschicht an einem in den gleichformigen Flussigkeitsstrom eingetauchten geraden Kreiszylinder, Dinglers Polytech. J. 326 (1911) 321–324.
[53] F. Homann, Der Einfluß großer Zähigkeit bei der Strömung um den Zylinder und um die Kugel, ZAMM - J. Appl. Math. Mech. /Zeitschrift Für Angewandte Mathematik Und Mechanik 16 (1936) 153–164, https://doi.org/10.1002/zamm.19360160304.
[54] L.J. Crane, Flow past a stretching plate, J. Appl. Math. Phys. (ZAMP) 21 (1970) 645–647, https://doi.org/10.1007/BF01587695.
[55] S. Goldstein, On backward boundary layers and flow in converging passages, J. Fluid Mech. 21 (1965) 33, https://doi.org/10.1017/S0022112065000034.
[56] C.Y. Wang, Liquid film on an unsteady stretching surface, Q. Appl. Math. 48 (1990) 601–610.

[57] A. Hamid, M.Khan Hashim, A. Hafeez, Unsteady stagnation-point flow of Williamson fluid generated by stretching/shrinking sheet with Ohmic heating, Int. J. Heat Mass Transf. 126 (2018) 933–940, https://doi.org/10.1016/j.ijheatmasstransfer.2018.05.076.
[58] Z. Uddin, K.S. Vishwak, S. Harmand, Numerical duality of MHD stagnation point flow and heat transfer of nanofluid past a shrinking/stretching sheet: metaheuristic approach, Chinese J. Phys. 73 (2021) 442–461, https://doi.org/10.1016/j.cjph.2021.07.018.
[59] U. Khan, A. Zaib, S. Abu Bakar, A. Ishak, Stagnation-point flow of a hybrid nanoliquid over a non-isothermal stretching/shrinking sheet with characteristics of inertial and microstructure, Case Stud. Therm. Eng. 26 (2021), 101150, https://doi.org/10.1016/j.csite.2021.101150.
[60] A. Yoshimura, R.K. Prud'homme, Wall slip corrections for couette and parallel disk viscometers, J. Rheol. (N Y N Y) 32 (1988) 53–67, https://doi.org/10.1122/1.549963.
[61] M.C. Sharatchandra, M. Sen, M. Gad-el-Hak, Thermal aspects of a novel viscous pump, J. Heat Transf. 120 (1998) 99–107, https://doi.org/10.1115/1.2830071.
[62] K.M. Bataineh, M.A. Al-Nimr, 2D navier–stokes simulations of microscale viscous pump with slip flow, J. Fluids Eng. 131 (2009), 051105, https://doi.org/10.1115/1.3112390.
[63] J. Nandal, S. Kumari, R. Rathee, The effect of slip velocity on unsteady peristalsis MHD blood flow through a constricted artery experiencing body acceleration, Int. J. Appl. Mech. Eng. 24 (2019) 645–659, https://doi.org/10.2478/ijame-2019-0040.
[64] A. Hamid, M. Khan, M. Alghamdi, Numerical simulation for transient flow of Williamson fluid with multiple slip model in the presence of chemically reacting species, HFF 29 (2019) 4445–4461, https://doi.org/10.1108/HFF-02-2019-0151.
[65] N.S. Wahid, N.M. Arifin, N.S. Khashi'ie, I. Pop, Hybrid nanofluid slip flow over an exponentially stretching/shrinking permeable sheet with heat generation, Mathematics 9 (2021) 30, https://doi.org/10.3390/math9010030.
[66] S. Abu Bakar, N.S. Wahid, N.M. Arifin, N.S. Khashi'ie, The flow of hybrid nanofluid past a permeable shrinking sheet in a Darcy–Forchheimer porous medium with second-order velocity slip, Waves in Random and Complex Media (2022) 1–18, https://doi.org/10.1080/17455030.2021.2020375.
[67] N.S. Khashi'ie, N.M. Arifin, I. Pop, R. Nazar, E.H. Hafidzuddin, N. Wahi, Three-dimensional hybrid nanofluid flow and heat transfer past a permeable stretching/shrinking sheet with velocity slip and convective condition, Chinese J. Phys. 66 (2020) 157–171, https://doi.org/10.1016/j.cjph.2020.03.032.
[68] E.H. Aly, I. Pop, MHD flow and heat transfer near stagnation point over a stretching/shrinking surface with partial slip and viscous dissipation: hybrid nanofluid versus nanofluid, Powder Technol. 367 (2020) 192–205, https://doi.org/10.1016/j.powtec.2020.03.030.
[69] S. Abu Bakar, N. Md Arifin, N.S. Khashi'ie, N. Bachok, Hybrid nanofluid flow over a permeable shrinking sheet embedded in a porous medium with radiation and slip impacts, Mathematics 9 (2021) 878, https://doi.org/10.3390/math9080878.
[70] W.-F. Xia, S. Ahmad, M.N. Khan, H. Ahmad, A. Rehman, J. Baili, T.N. Gia, Heat and mass transfer analysis of nonlinear mixed convective hybrid nanofluid flow with multiple slip boundary conditions, Case Stud. Therm. Eng. 32 (2022), 101893, https://doi.org/10.1016/j.csite.2022.101893.
[71] W. Cao, A. I.L., S.-.J. Yook, O. V.A., X. Ji, Simulation of the dynamics of colloidal mixture of water with various nanoparticles at different levels of partial slip: ternary-hybrid nanofluid, Int. Commun. Heat and Mass Transf. 135 (2022) 106069. 10.1016/j.icheatmasstransfer.2022.106069.
[72] N.A.A.M. Nasir, A. Ishak, I. Pop, Stagnation point flow and heat transfer past a permeable stretching/shrinking Riga plate with velocity slip and radiation effects, J. Zhejiang Univ. Sci. A. 20 (2019) 290–299, https://doi.org/10.1631/jzus.A1800029.
[73] N.S. Khashi'ie, N.M. Arifin, I. Pop, N.S. Wahid, Effect of suction on the stagnation point flow of hybrid nanofluid toward a permeable and vertical Riga plate, Heat Transf. 50 (2021) 1895–1910, https://doi.org/10.1002/htj.21961.
[74] K. Bhattacharyya, S. Mukhopadhyay, G.C. Layek, Slip effects on boundary layer stagnation-point flow and heat transfer towards a shrinking sheet, Int. J. Heat Mass Transf. 54 (2011) 308–313, https://doi.org/10.1016/j.ijheatmasstransfer.2010.09.041.
[75] S. Mukhopadhyay, H.I. Andersson, Effects of slip and heat transfer analysis of flow over an unsteady stretching surface, Heat Mass Transf. 45 (2009) 1447–1452, https://doi.org/10.1007/s00231-009-0516-7.
[76] B. Takabi, S. Salehi, Augmentation of the heat transfer performance of a sinusoidal corrugated enclosure by employing hybrid nanofluid, Adv. Mech. Eng. 6 (2015), 147059, https://doi.org/10.1155/2014/147059.
[77] C.J. Ho, W.K. Liu, Y.S. Chang, C.C. Lin, Natural convection heat transfer of alumina-water nanofluid in vertical square enclosures: an experimental study, Int. J. Therm. Sci. 49 (2010) 1345–1353, https://doi.org/10.1016/j.ijthermalsci.2010.02.013.
[78] M.A. Sheremet, I. Pop, A.V. Rosca, The influence of thermal radiation on unsteady free convection in inclined enclosures filled by a nanofluid with sinusoidal boundary conditions, HFF 28 (2018) 1738–1753, https://doi.org/10.1108/HFF-09-2017-0375.
[79] N. Ahmed, A. Tassaddiq, R. Alabdan, U.Khan Adnan, S. Noor, S.T. Mohyud-Din, I. Khan, Applications of nanofluids for the thermal enhancement in radiative and dissipative flow over a wedge, Appl. Sci. 9 (2019) 1976, https://doi.org/10.3390/app9101976.
[80] R. Ul Haq, N.F.M. Noor, Z.H. Khan, Numerical simulation of water based magnetite nanoparticles between two parallel disks, Adv. Powder Technol. 27 (2016) 1568–1575, https://doi.org/10.1016/j.apt.2016.05.020.
[81] J.H. Merkin, On dual solutions occurring in mixed convection in a porous medium, J. Eng. Math. 20 (1986) 171–179, https://doi.org/10.1007/BF00042775.
[82] P.D. Weidman, D.G. Kubitschek, A.M.J. Davis, The effect of transpiration on self-similar boundary layer flow over moving surfaces, Int. J. Eng. Sci. 44 (2006) 730–737, https://doi.org/10.1016/j.ijengsci.2006.04.005.
[83] S.D. Harris, D.B. Ingham, I. Pop, Mixed convection boundary-layer flow near the stagnation point on a vertical surface in a porous medium: brinkman model with slip, Transp. Porous. Med. 77 (2009) 267–285, https://doi.org/10.1007/s11242-008-9309-6.
[84] N.S. Khashi'ie, N. Md Arifin, I. Pop, Mixed convective stagnation point flow towards a vertical Riga plate in hybrid Cu-Al2O3/water nanofluid, Mathematics 8 (2020) 912, https://doi.org/10.3390/math8060912.
[85] A. Malvandi, F. Hedayati, D.D. Ganji, Nanofluid flow on the stagnation point of a permeable non-linearly stretching/shrinking sheet, Alexandria Eng. J. 57 (2018) 2199–2208, https://doi.org/10.1016/j.aej.2017.08.010.
[86] A. Mishra, M. Kumar, Velocity and thermal slip effects on MHD nanofluid flow past a stretching cylinder with viscous dissipation and Joule heating, SN Appl. Sci. 2 (2020) 1350, https://doi.org/10.1007/s42452-020-3156-7.
[87] K. Apmann, R. Fulmer, A. Soto, S. Vafaei, Thermal conductivity and viscosity: review and optimization of effects of nanoparticles, Materials (Basel) 14 (2021) 1291, https://doi.org/10.3390/ma14051291.